Acid-denatured small heat shock protein HdeA from *Escherichia coli* forms reversible fibrils with an atypical secondary structure

Received for publication, August 28, 2018, and in revised form, December 6, 2018 Published, Papers in Press, December 10, 2018, DOI 10.1074/jbc.RA118.005611

Shiori Miyawaki[‡], **Yumi Uemura**[§], **Kunihiro Hongo**[‡§¶], **Yasushi Kawata**[‡§¶], **and Tomohiro Mizobata**[‡§¶1]

From the [‡]*Graduate School of Sustainability Science,* [§]*Department of Engineering, and* [¶]*Center for Research on Green Sustainable Chemistry, Tottori University, Tottori 680-8552, Japan*

Edited by Paul E. Fraser

The periplasmic small heat shock protein HdeA from *Escherichia coli* is inactive under normal growth conditions (at pH 7) and activated only when *E. coli* cells are subjected to a sudden decrease in pH, converting HdeA into an acid-denatured active state. Here, using *in vitro* fibrillation assays, transmission EM, atomic-force microscopy, and CD analyses, we found that when HdeA is active as a molecular chaperone, it is also capable of forming inactive aggregates that, at first glance, resemble amyloid fibrils. We noted that the molecular chaperone activity of HdeA takes precedence over fibrillogenesis under acidic conditions, as the presence of denatured substrate protein was sufficient to suppress HdeA fibril formation. Further experiments suggested that the secondary structure of HdeA fibrils deviates somewhat from typical amyloid fibrils and contains α-helices. Strikingly, HdeA fibrils that formed at pH 2 were immediately resolubilized by a simple shift to pH 7 and from there could regain molecular chaperone activity upon a return to pH 1. HdeA, therefore, provides an unusual example of a "reversible" form of protein fibrillation with an atypical secondary structure composition. The competition between active assistance of denatured polypeptides (its "molecular chaperone" activity) and the formation of inactive fibrillary deposits (its "fibrillogenic" activity) provides a unique opportunity to probe the relationship among protein function, structure, and aggregation in detail.

Pathogenic *Escherichia coli* strains must be resistant to the highly acidic environment of the stomach to successfully infect their human host (1). A major contributor to this acid resistance is expressed in the form of two structurally homologous but functionally distinct periplasmic small heat shock proteins, HdeA and HdeB (2–7). The two chaperones are initially translated as precursors (HdeA, 110 amino acids; HdeB, 108 amino acids) (8) that are transported to the periplasm and then processed to mature forms (HdeA, 89 residues; HdeB, 79 residues). At neutral pH, both HdeA and HdeB form inert, α-helix–rich dimers (exemplified for HdeA in Fig. 7) (4). However, HdeA and HdeB both undergo acid-induced denaturation at low pH (<pH 3 for HdeA; <pH 4 for HdeB), upon which these two proteins become active molecular chaperones, capable of binding to a broad range of polypeptides that are denatured and are therefore susceptible to aggregation (2, 6, 9). Due to differences in structure and molecular interactions with targets, the conditions under which HdeA and HdeB are optimally functional are different; HdeA functions best at pH 2, whereas HdeB is optimally active at pH 4 (7). This difference translates to a separation of roles between the two small heat shock proteins that are reflected in their chaperone-client specificities (10). Apparently, the mechanism by which HdeA and HdeB prevents aggregation of periplasmic targets is through simple binding and release, as no additional molecular mechanisms, such as ATPase activity or specific cofactor-binding sites, have been implicated so far (7, 11–13).

In an effort analogous to our previous studies to use bacterial chaperones for protein aggregation control (14, 15), we set out to probe the possibilities of using HdeA and HdeB in the control of irreversible aggregation and fibrillation of proteins, specifically at low pH. We began our experiments using human α-Synuclein because previous studies by Uversky *et al.* (16) demonstrated that this protein forms fibrils more readily at lower pH (pH <5) than at neutral pH (Fig. 1). Surprisingly, from these preliminary experiments we found that HdeA itself, in its acid-denatured active form, was capable of forming fibril-like deposits that shared numerous characteristics with pathological amyloid fibrils, such as binding to the Thioflavin-T (Thio-T)[2] fluorescent probe (17) and regular twisted fibril morphologies that were observable by transmission EM (TEM) and atomic-force microscopy (AFM).

We describe here our findings regarding the fibril-forming abilities of HdeA and the relationship between this ability and the function of HdeA as an acid-induced molecular chaperone. A very surprising finding was that once formed, these HdeA fibrils could be reconstituted through a simple shift to neutral pH and regain molecular chaperone activity. Our findings highlight the remarkable reversibility of the structural transitions of HdeA and the suitability of using HdeA as an attractive exper-

This work was partially supported by Tottori University, Japan Agency for Medical Research and Development (AMED) Grant JP18dm0107073 and the Skylark Food Science Institute. The authors declare that they have no conflicts of interest with the contents of this article.

This article contains Figs. S1–S3 and Table S1.

[1] To whom correspondence should be addressed: Dept. of Engineering, Tottori University, 4-101 Koyama-Minami, Tottori City, Tottori 680-8552 Japan. Tel./Fax: 81-857-31-5691; E-mail: mizobata@tottori-u.ac.jp.

[2] The abbreviations used are: Thio-T, Thioflavin-T; ADH, alcohol dehydrogenase; AFM, atomic-force microscopy; ATR, attenuated total reflection; TEM, transmission electron microscopy.

© 2019 Miyawaki et al. Published under exclusive license by The American Society for Biochemistry and Molecular Biology, Inc.

Downloaded from http://www.jbc.org/ at TOTTORI UNIVERSITY on February 11, 2019

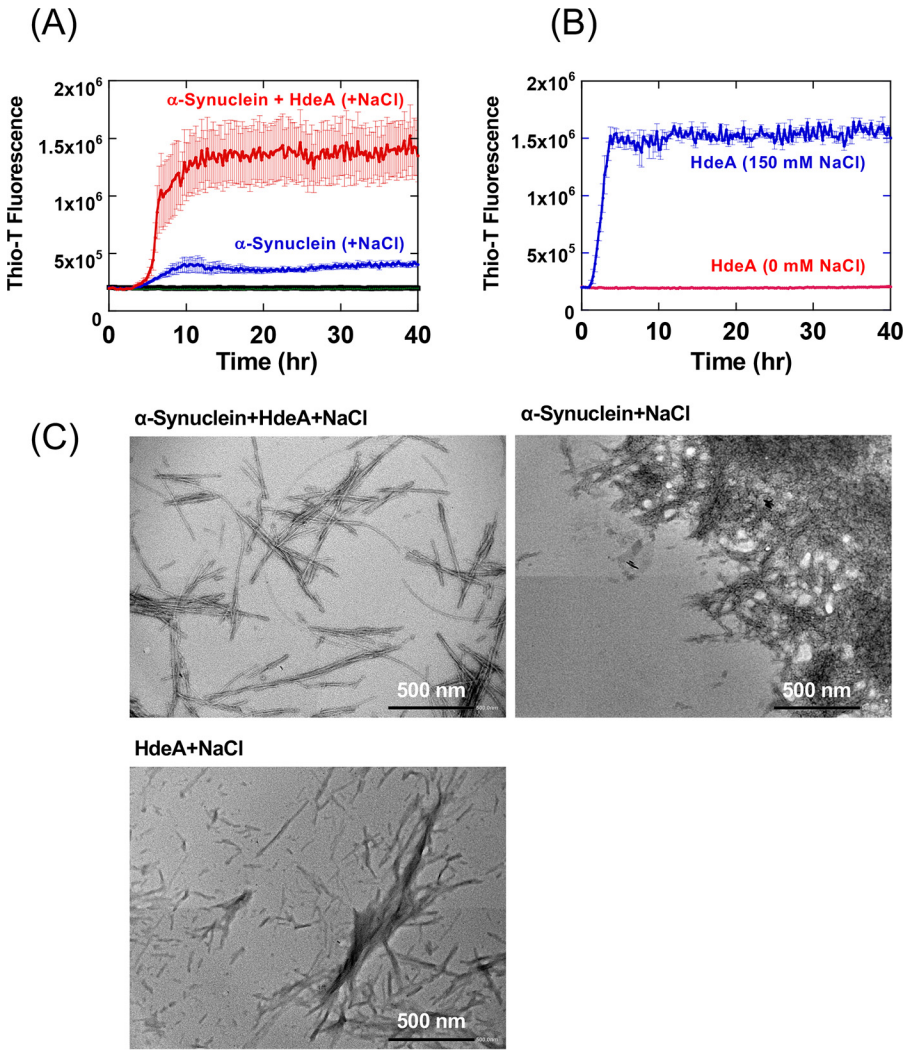

Figure 1. HdeA is capable of forming fibril-like deposits at low pH. *Error bars* represent S.E. derived from averages of three samples. *A*, *in vitro* fibrillation of α-Synuclein and HdeA samples incubated at pH 2.0. Experiments were performed in 20 mM glycine-HCl buffer containing 20 μM Thioflavin-T. Samples denoted "+*NaCl*" indicate experiments performed with the above buffer containing 150 mM NaCl. The *green* trace represents α-Synuclein + HdeA incubated at pH 2.0 without NaCl, and the *black* trace (overlapping the *green* trace) represents α-Synuclein incubated at pH 2.0 without NaCl. *B*, fibrillation of HdeA samples at pH 2.0. *C*, transmission electron micrographs of negatively stained fibril samples taken from experiments in *A* and *B*. *Scale bars* indicate 500 nm.

imental system to probe the relationship between protein structural dynamism and activity.

Results

Our original intent was to see whether HdeA was capable of suppressing fibrillation of α-Synuclein (16). However, as shown in Fig. 1*A*, contrary to our expectations the addition of HdeA to a sample of α-Synuclein incubated at pH 2.0 caused a large increase in Thio-T–binding fluorescence compared with samples containing α-Synuclein only. This prompted us to probe in more detail the behavior of HdeA at low pH in isolation, which revealed this protein's ability to form similar insoluble fibrils. Fig. 1*B* shows a typical fibril-forming reaction of HdeA at pH 2.0, monitored by Thio-T fluorescence. The reaction proceeded according to a mechanism with an initial lag phase where no increase in fluorescence was observed followed by a rapid increase in fluorescence that reflected the extension phase. The Thio-T fluorescence intensities attributed to the formation of fibrils were stronger in the presence of 150 mM NaCl, and experiments in the absence of NaCl showed no increases in Thio-T fluorescence intensity (Fig. 1*B*, *red*). However, subsequent experiments showed that this lack of fluorescence signal increase was not due to the absence of fibrils but to differences in fibril morphology that altered the sensitivity to Thio-T, as probed in detail in Fig. 3*A*.

Each of the samples in Fig. 1, *A* and *B*, that displayed increases in Thio-T fluorescence intensity were confirmed for the presence of actual fibrillar deposits by negatively stained TEM analysis (Fig. 1*C*). Fibrils observed for the α-Synuclein + HdeA samples consisted mainly of short, densely stained fibrils mixed with longer, thinner twisted fibrils. In contrast, fibrils of α-Synuclein formed at pH 2.0 without HdeA consisted mainly of short fibril clumps. Finally, fibrils of HdeA were short, rod-like fibrils that showed a tendency to aggregate into larger deposits.

Having established that HdeA was capable of forming fibrillar aggregates at low pH, we next probed the sensitivity of this reaction to various experimental parameters. We first observed

Downloaded from http://www.jbc.org/ at TOTTORI UNIVERSITY on February 11, 2019

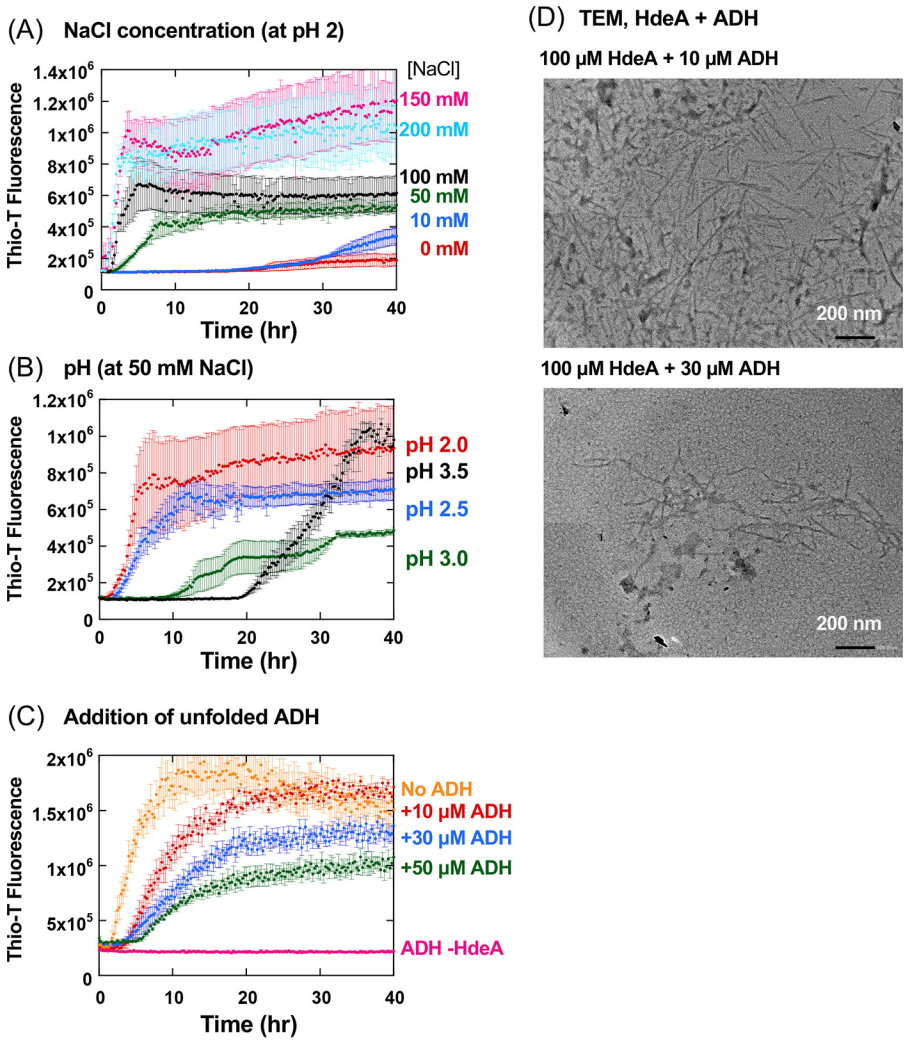

Figure 2. Sensitivity of HdeA fibrillogenesis to various experimental parameters. The differences in experimental parameters are color-coded and shown to the *right* of each panel. *Error bars* represent S.E. derived from averages of three samples. *A*, fibril-forming reaction of HdeA at pH 2 in the presence of various concentrations of NaCl. Samples were subjected to intermittent shaking followed by fluorescence measurement in a PerkinElmer Life Sciences ARVO plate reader. *B*, fibril-forming reaction of HdeA at 50 mM NaCl and various pH values. *C*, addition of denatured ADH to the HdeA fibrillation reaction prevents fibril formation. Samples of HdeA (100 μM) were incubated at pH 1.0 in the presence of increasing concentrations of ADH predenatured under the same conditions. Samples containing only denatured ADH (*pink*) displayed no increases in Thio-T fluorescence. *D*, TEM images of selected samples from *C*.

a strong dependence of HdeA fibrillation on the concentration of NaCl (Fig. 2*A*). At low NaCl concentrations, HdeA fibrils were formed through an extended lag phase followed by a modest increase in Thio-T fluorescence. In the presence of higher concentrations of NaCl, HdeA fibrils formed much more rapidly, and a very strong increase in fluorescence intensity exemplified the extension phase.

Because the results suggested that HdeA formed fibrils from its active acid-unfolded state, we wished to determine whether this fibril transformation was indeed correlated to the acid unfolding of HdeA. Previous experiments have shown that the native structure of HdeA undergoes denaturation at solvent conditions between pH 2.2 and pH 4.0, with transition midpoint pH values slightly lower than 3 (for secondary structure monitored by CD (9)) or 3.5 (for dimer dissociation monitored by FRET (11)). Therefore, we performed fibril-forming assays at various pH conditions centered around this pH region. As shown in Fig. 2*B*, HdeA tended to form fibrils rapidly at pH conditions below 3.0. An extension of the lag phase of fibrillation and a decrease in the final Thio-T fluorescence value were both observed at pH conditions higher than 3.0. We also noted that the average trace of fibril formation at pH 3.0 became rather erratic and apparently multistage in nature. However, we found that this was caused by the fact that individually prepared samples of HdeA displayed large variances in lag-phase intervals (Fig. S1). These variances in lag phase caused an artifact in the averaged trace.

The results in Fig. 2*B* demonstrated that HdeA formed fibrils under conditions where this protein was active as a molecular chaperone, *e.g.* at pH values lesser than 3. We were therefore curious to determine whether these two tendencies, fibrillogenesis and molecular chaperone activity, were mutually exclusive, so we performed fibril extension experiments in the presence of a model unfolded target protein, yeast alcohol dehydrogenase (ADH) at pH 1.0. As seen in Fig. 2*C*, the addition of increasing concentrations of acid-denatured ADH served to strongly suppress the fibril formation of HdeA at this pH, suggesting that the molecular chaperone activity of HdeA took precedence

Downloaded from http://www.jbc.org/ at TOTTORI UNIVERSITY on February 11, 2019

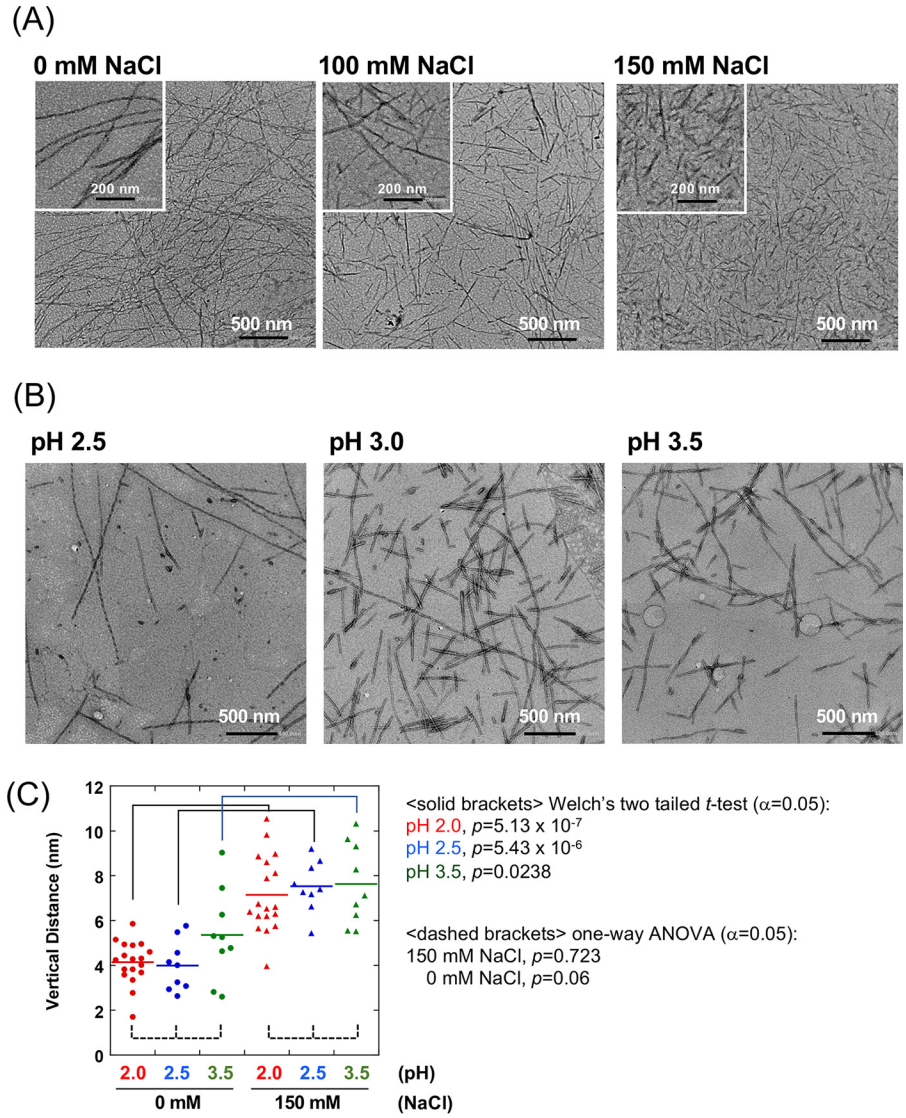

Figure 3. TEM and AFM analysis of HdeA fibrils. *A*, TEM analysis of HdeA fibrils formed at pH 2.0 in the presence of different NaCl concentrations. *Magnification* was ×15,000. The *inset* in each panel shows images of the same sample taken at higher magnification (×30,000). *B*, TEM analysis of HdeA fibrils formed at various pH values in the absence of NaCl. *C*, scatter column plots of vertical height measurements of HdeA fibrils formed under various NaCl concentrations and pH values. *Horizontal lines* in the figure indicate the mean height value for each experimental condition. Vertical height measurements were taken from AFM images such as those shown in Fig. S2. The number of measurements taken were $n = 18$ for samples formed at pH 2.0 and $n = 9$ for samples formed at other pH conditions. Measurements of samples formed at a given pH in the presence and absence of NaCl were compared using Welch's two-tailed *t* test (*solid brackets*) to determine whether the height of the fibrils differed when formed at different NaCl concentrations (*p* values are given next to the main figure). Additionally, measurements for the three samples formed in the presence of a given NaCl concentration were compared using one-way analysis of variance (*ANOVA*) (*dashed brackets*) to determine whether the average height of fibrils formed in the presence of a given NaCl concentration was statistically indistinguishable in thickness regardless of the pH. Taken together, both statistical analyses supported our notion that the height (thickness) of the HdeA fibrils formed depended on the NaCl concentration during the experiment but not on the pH.

over the formation of fibrils when target proteins were present. This suppression of fibrils was also reflected in TEM images of HdeA samples formed in the presence of denatured ADH (Fig. 2*D*) where we generally observed less fibrillar structures when the concentration of denatured ADH was increased.

To characterize the morphological characteristics of HdeA fibrils under the conditions probed in Fig. 2, we next performed TEM and AFM characterization of HdeA fibrils. We found that the fibril morphology of HdeA was quite sensitive to NaCl concentration. Fibrils of HdeA formed in low concentrations of NaCl tended to form long, thin filaments, whereas in the presence of high concentrations of NaCl, HdeA fibrils tended toward shorter and thicker rodlike forms (Fig. 3*A*). In contrast, HdeA fibrils that were formed at a certain NaCl concentration were relatively indifferent to the pH conditions where fibrillation occurred; for example, as seen in Fig. 3*B*, we could not detect any large differences in morphology in fibrils formed in the absence of NaCl at various pH values. This visual impression was confirmed in more quantitative analyses that utilized AFM. As shown in Fig. 3*C*, the thicknesses (as measured by the vertical height difference of fibrils probed on mica by AFM; individual AFM images are shown in Fig. S2) of fibrils formed at a given NaCl concentration was statistically indistinguishable regardless of the pH in which the fibrils were formed. However, when we compared the dimensions of fibrils formed in the presence of 150 mM NaCl with those formed in the absence of NaCl,

Downloaded from http://www.jbc.org/ at TOTTORI UNIVERSITY on February 11, 2019

we found that the former were significantly thicker at each pH that we tested.

From the results in Figs. 2 and 3, we may conclude that HdeA tends to form fibrils when the original structure is perturbed to expose a putative interface where fibril seed nucleation and subsequent fibril extension may proceed. The presence of NaCl served to shorten the initial lag time required for fibril nucleus formation, suggesting that HdeA fibrillation was dependent partially on either ionic shielding or enhancement of hydrophobic effects caused by an increase in ionic strength. NaCl may act to change the interactions between HdeA molecules during fibrillation, which are translated to differences in fibril morphology.

Because the molecular chaperone activity of HdeA depends on the acid denaturation of its native structure, we were curious to determine whether sudden changes in pH would affect the fibril-forming reaction of HdeA in a similar manner. To this end, we probed the effects of shifting the pH of HdeA fibril samples that had been formed at pH 2.0 to higher values. Interestingly, incubating HdeA fibrils that were formed at pH 2 at higher pH resulted in decreases in Thio-T fluorescence (Fig. 4*A*). The degree of signal decrease depended on the incubation pH; fluorescence intensities were unchanged after a pH shift to 4.6, but a partial decrease in intensity occurred upon a shift to pH 5.6, and complete loss of signal was observed at pH values higher than 6.0. The loss of fibrillar forms after incubation at pH 7 was confirmed in TEM images as shown in Fig. 4*B*. SDS-PAGE analysis of the reconstituted fibrils (Fig. 4*C*) showed that the insoluble fibrils formed at pH 2 (Fig. 4*C*, *lane group c*) were largely shifted to the soluble fraction by the shift in pH (Fig. 4*C*, *lane group d*). Strikingly, the HdeA samples that were recovered after incubation at pH 7 were active as molecular chaperones when reintroduced to low pH conditions as assayed using ADH (Fig. 4*D*, compare *lane groups b* and *d*). The data in Fig. 4 suggested strongly that the formation of HdeA fibrils at low pH was reversible and that HdeA was capable of converting freely between inactive dimer (neutral pH) and two very different low-pH structural forms, active monomer and insoluble fibril.

To probe the details of the structural transitions between native dimer, inactive fibril, and resolubilized HdeA, we performed spectral analysis aimed at determining the secondary structural characteristics of each HdeA form. CD spectra of representative fibril samples (Fig. 5*A*) revealed that the CD spectra of HdeA fibrils formed at pH 2.0 diverged somewhat from typical amyloid fibrils, such as fibrils of α-Synuclein (Fig. 5*A*, *magenta*). An analysis of the CD spectra using an online tool (BeStSel) (18) suggested that the HdeA fibrils contained significant fractions of α-helical content (Fig. S3 and Table S1). HdeA fibrils that had been resolubilized by a shift in pH to 7.0 (Fig. 5*B*) closely resembled the spectra for the native HdeA dimer regardless of the initial salt conditions used for the fibrillation reaction, suggesting that HdeA was indeed capable of reversibly returning to a state resembling its initial native conformation.

As we were interested in determining the process by which HdeA fibrils were formed at low pH, we next probed the changes in CD spectra that occur during formation of fibrils (Fig. 5*C*) both in the presence (150 mM) and absence of NaCl. In the absence of NaCl, we observed a slow change in the CD spectra of HdeA over the course of several days. No intermediate states during this transition were immediately apparent. In contrast, the CD spectra of HdeA in the presence of 150 mM NaCl initially transitioned from a spectrum resembling an acid-denatured state to one with a strong negative absorbance at 216 nm, which subsequently shifted again to a spectrum with a smaller negative absorbance with a minimum at 218 nm. This result suggested that formation of HdeA fibrils in the presence of 150 mM NaCl involved at least one intermediate conformation.

To obtain additional information regarding the secondary structure of HdeA fibrils at pH 2 and pH 7, we used attenuated total reflection (ATR)-FTIR spectroscopy to monitor the Amide I band of lyophilized HdeA samples hydrated with deuterium oxide (D_2O). As seen in Fig. 6*A*, the IR absorbance spectra of native HdeA showed a peak in the vicinity of 1640 cm^{-1} and resembled the spectra of the α-helical–rich protein lysozyme, whereas spectra of the fibrils displayed a peak at ~1625 cm^{-1} and resembled the spectra of α-chymotrypsin, a protein with high β content (19). A closer look using second derivative analysis of the absorbance spectra provided more details. All of the absorbance spectra measured showed absorption bands at 1652 and 1642 cm^{-1}, which are both characteristic absorption bands of α-helix (19). The spectra of native HdeA displayed a band at 1637 cm^{-1} that was not seen in the other samples, which may be attributed to random structure; in contrast, all of the samples with the exception of native HdeA and the fibril form of HdeA formed in 0 mM NaCl displayed a prominent band at 1634 cm^{-1}, which is characteristic of β-sheet (19). These results support the idea that fibrils of HdeA contain significant amounts of both α-helical and β-sheet secondary structure.

This hybrid nature of HdeA fibrils was highlighted further when compared with the second derivative spectra of native HdeA and α-Synuclein fibrils (Fig. 6*B*). Unlike native HdeA, with prominent absorption bands at 1660–1640 cm^{-1}, or α-Synuclein, with strong absorption bands observed between 1640 and 1620 cm^{-1}, the second derivative spectra of HdeA fibrils formed in the presence of 150 mM NaCl showed observable peaks in both of these regions.

Interestingly, the IR spectra of HdeA fibril samples formed at pH 2 and subsequently reconstituted at pH 7.0 resembled neither the spectra of native HdeA nor the spectra of the original fibril form (Fig. 6*C*). Notably, we observed significant differences mainly in the 1640–1620 cm^{-1} region that may be attributed to incubation at pH 7. These differences may be suggestive of a soluble state that is distinct from the original native structure of HdeA that is formed by fibrillation at pH 2 and subsequent reconstitution at pH 7, which is in apparent conflict with the results seen in the CD spectra (Fig. 5*B*) that suggested that HdeA fully recovered the secondary structure of its native form.

Discussion

The small heat shock proteins HdeA and HdeB are an important component of the acid-resistance mechanism in Gram-negative bacteria (20). *E. coli* strains that do not express these molecular chaperones have been demonstrated to be highly

Downloaded from http://www.jbc.org/ at TOTTORI UNIVERSITY on February 11, 2019

ASBMB

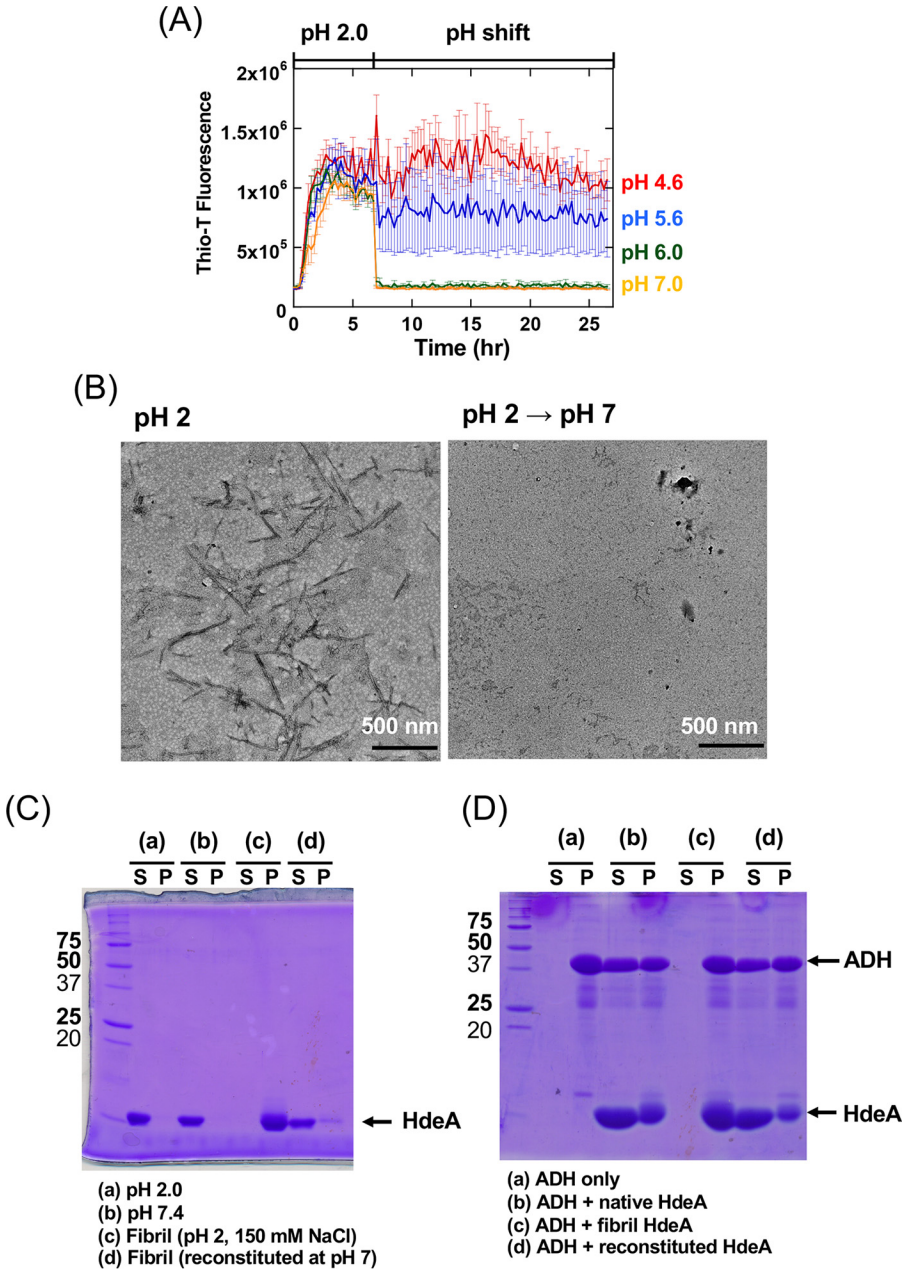

Figure 4. Reversibility of the HdeA fibril-forming reaction. *A*, changes in Thio-T fluorescence intensity upon a shift from pH 2 to various higher pH values. *Error bars* represent S.E. derived from averages of three samples. The experiment was initiated at pH 2.0, and at the time point indicated above the graph, samples were adjusted to the new pH value by addition of aliquots of Tris base solution (see "Experimental procedures"). *B*, TEM micrographs of HdeA fibril samples before and after pH shift to 7.0. *C*, partitioning of various HdeA samples to soluble and insoluble fractions. *S*, soluble fraction; *P*, precipitate fraction. *Lane group a*, HdeA adjusted to pH 2.0 and immediately analyzed (the acid-unfolded state); *lane group b*, HdeA in buffer at pH 7.4 (native HdeA); *lane group c*, HdeA fibrils formed at pH 2.0 by shaking; *lane group d*, HdeA fibrils formed at pH 2 and incubated at pH 7.0 (reconstituted fibrils). *D*, HdeA fibril samples shifted to pH 7.0 are capable of being reactivated as molecular chaperones at pH 1.0. *S*, soluble fraction; *P*, precipitate fraction. Samples are from *left*: *lane group a*, ADH incubated at pH 1.0; *lane group b*, ADH and native HdeA incubated at pH 1.0; *lane group c*, ADH and HdeA fibrils (formed at pH 2.0) incubated at pH 1.0; *lane group d*, ADH and HdeA fibrils (formed at pH 2.0 and then shifted to pH 7.0) incubated at pH 1.0.

sensitive to acidic conditions (2, 4). The inherent "environmentally sensitive" nature of these small heat shock proteins is a novel and interesting characteristic in the molecular chaperone mechanism of HdeA/HdeB, and similar "conditionally active" molecular chaperones are currently an interesting subject of study.

In this study we have found that, in addition to becoming a promiscuous molecular chaperone upon denaturation at low pH, HdeA displays a tendency to form insoluble fibrillar aggregates that were morphologically similar to amyloid fibrils, the irreversible protein deposits that are implicated in many neurological disorders. The kinetics of this reaction is sensitive to the pH of the experiment, and the morphological aspects of the reaction are sensitive to the ionic strength. Generally, the tendency toward rapid fibril formation seems to be stronger at lower pH and higher salt concentrations; however, the resultant fibrils are relatively short and rodlike. Contrariwise, although both the rate and lag time of fibrillation at higher pH and lower

Downloaded from http://www.jbc.org/ at TOTTORI UNIVERSITY on February 11, 2019

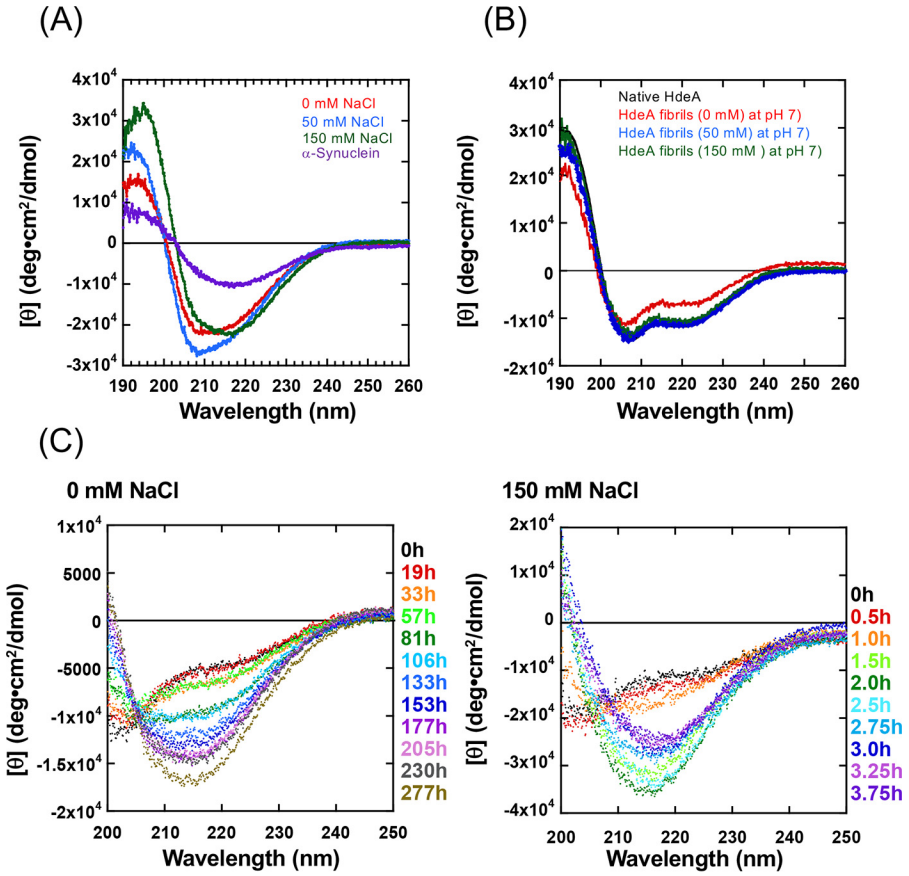

Figure 5. CD analysis of HdeA. *A*, CD spectra of HdeA fibrils formed at pH 2.0 and various concentrations of NaCl. *B*, CD spectra of native HdeA and HdeA fibrils that were first formed at pH 2.0 and various NaCl concentrations and then shifted to pH 7.0. *C*, time-lapse scans of HdeA samples incubated at pH 2.0 and the indicated concentration of NaCl. The time point of each spectrum is indicated in color to the *right* of each panel. *deg*, degrees.

NaCl concentrations reflect a more gradual fibrillation process, the resultant HdeA fibrils are longer, filament-like structures.

Although morphologically similar and detectable with Thio-T, an amyloid-specific fluorescence probe, we have found that fibrils formed from acid-denatured HdeA deviated somewhat from common characteristics of other, typical amyloid fibrils in their CD spectra (Fig. 5). Compared with spectra of α-Synuclein fibrils, which displayed a clear absorbance minimum at 218 nm, the CD spectra of HdeA fibrils all displayed minor absorbances at shorter wavelengths. Estimation of the secondary structural content (Fig. S3 and Table S1) suggested that the fibrils might contain significant amounts of α-helical content. This is an unusual characteristic to detect in fibrils, although not entirely unknown, as seen previously for helix-turn-helix peptides derived from apolipoprotein A-I (21) as well as the bacterially secreted phenol-soluble modulin PSMα3, recently determined in crystallography analysis as a fibril with amphipathic cross-α structure (22). Considering the activity of HdeA as molecular chaperone under these conditions, it is quite possible that the denatured HdeA polypeptide retains a considerable amount of α-helical structure even when incorporated into fibrils, and only a crucial localized segment of the amino acid sequence is required to form the Thio-T–reactive fibril interface. We would like to add, however, that the estimation of α-helical content of HdeA fibrils by BeStSel was abnormally high, exceeding 50%. Secondary structure estimation of proteins by BeStSel is sensitive to small differences in protein concentration and cell pathlength (per the "Information" section of the BeStSel website), and the values shown in Table S1 may be overestimating the actual secondary structure content of the samples. ATR-FTIR spectra of HdeA fibrils (Fig. 6) in D_2O displayed a characteristic IR absorption band centered at 1637 cm^{-1}, indicative of β-sheet structures, so the question of the accurate secondary structural content of HdeA fibrils remains open for further experimentation.

The differences in fibril morphology that could be attained by modulating the NaCl concentration of the sample suggested that there may be multiple HdeA forms that are fibrillogenic and lead to different structural forms. This idea was supported by results in Fig. 5*C*, which demonstrated that, at least in the presence of 150 mM NaCl, HdeA formed fibrils via at least one intermediate state that was distinguishable by CD spectral analysis. The idea that HdeA forms morphologically diverse fibrils through distinct intermediate states that are formed according to different experimental conditions needs to be probed further.

The path toward HdeA fibril formation was demonstrated to be in competition with the role of molecular chaperone, and we have found that the two pathways are mutually exclusive; HdeA is incapable of acting as a molecular chaperone in the fibril state, and the presence of unfolded proteins such as ADH prevents this chaperone from attaining the inactive fibril form. A

Downloaded from http://www.jbc.org/ at TOTTORI UNIVERSITY on February 11, 2019

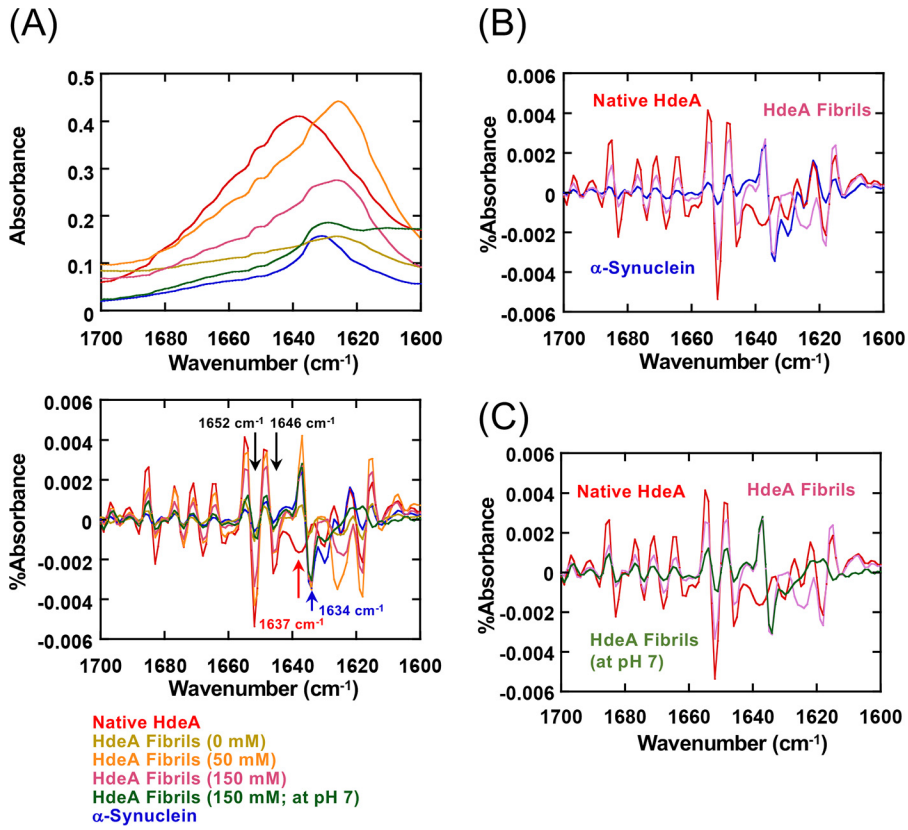

Figure 6. ATR-FTIR analysis of HdeA. *A*, absorption spectra of the Amide I band of HdeA samples. The *upper panel* indicates the absorbance spectra, and the *lower panel* indicates the second derivative spectra. Each trace is color-coded according to the legend shown below the panels. In the *lower panel*, the wavenumber values noted in *black* represent absorption bands that were observed in all of the samples measured (1652 and 1646 cm^{-1}), and the absorption band noted in *red* is a band that was observed only for the native HdeA sample (1637 cm^{-1}). The absorption band in *blue* notes an absorption band (1634 cm^{-1}) that was observed in all of the samples except for native HdeA and HdeA fibril samples formed at 0 mM NaCl. *B*, comparison of the second derivative spectra of HdeA fibrils with native HdeA, which is rich in α-helix, and α-Synuclein fibrils, representing a sample with high β-sheet content. The color legend follows the convention used in *A*. *C*, comparison of the second derivative spectra of three HdeA forms characterized in the present study. The color legend follows the convention used in *A*. Prominent differences are seen in the region spanning 1640–1620 cm^{-1}.

simple explanation for this result would be that the molecular interfaces for both molecular chaperone activity and fibrillogenesis either overlap or interact with each other so that simultaneous attainment of both states is impossible. However, prediction algorithms for amyloid core regions also highlight the possibilities of a more complex mechanism. When we submitted the amino acid sequence of HdeA to an online site that utilizes and compares multiple algorithms to predict potential amyloidogenic sequence regions (http://aias.biol.uoa.gr/AMYLPRED2/)[3] (23), we found a total of three sequence "hot spots" that were flagged by a plurality of prediction algorithms as potential amyloid core regions (sequences are highlighted when more than 5 of the 11 algorithms provided flag the sequence region as "amyloidogenic") (Fig. 7). The sequence region with the most "hits," corresponding to residues 52–59 (VQGIATVT) in the HdeA amino acid sequence, includes two valine residues that have been identified as residues that are necessary for the molecular chaperone activity of HdeA (Val^{52} and Val^{58} (24); diverting this sequence region to fibrils would likely serve to prevent HdeA from interacting with denatured protein targets. The presence of two other, lesser flagged sequence regions (^{32}AVGFA^{36} and ^{61}AIVQA(C)T^{67}; the C is not flagged) is interesting when we consider the multiple morphologies that HdeA fibrils have displayed in our experiments. We note also with interest that the three putative fibrillogenic sequence regions may be mapped to two diverse locations in the native HdeA structure at pH 7; ^{32}AVGFA^{36} is located at the dimer interface, whereas the other two sequences are exposed sections at the outer sides of the dimer (Fig. 7). The sequence region ^{32}AVGFA^{36} is potentially very interesting when we consider that our experiments suggest that the formation of HdeA fibrils depends on a structural transition that occurs at pH ~3 (Fig. 2*B*), whereas the dissolution of this fibril structure occurs at pH values greater than 4.6 (Fig. 4*A*). A recent study by Salmon *et al.* (25) explored the detailed process of HdeA acid denaturation as monitored by intrinsic tryptophan fluorescence and NMR. The authors' results using intrinsic fluorescence suggested that the acid denaturation of HdeA proceeded through two distinct transitions, the first transition occurring at a midpoint pH of 5.56 and a second transition at pH 2.81. These two transition midpoints correlate rather strongly to the dissolution and formation of HdeA fibrils, respectively, in our experiments. It should be noted that Salmon *et al.* (25) determined that the transition occurring at a midpoint pH of 5.56 involved the

[3] Please note that the JBC is not responsible for the long-term archiving and maintenance of this site or any other third party hosted site.

Downloaded from http://www.jbc.org/ at TOTTORI UNIVERSITY on February 11, 2019

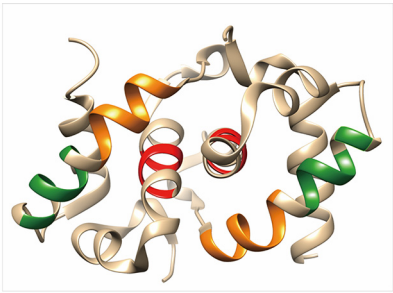

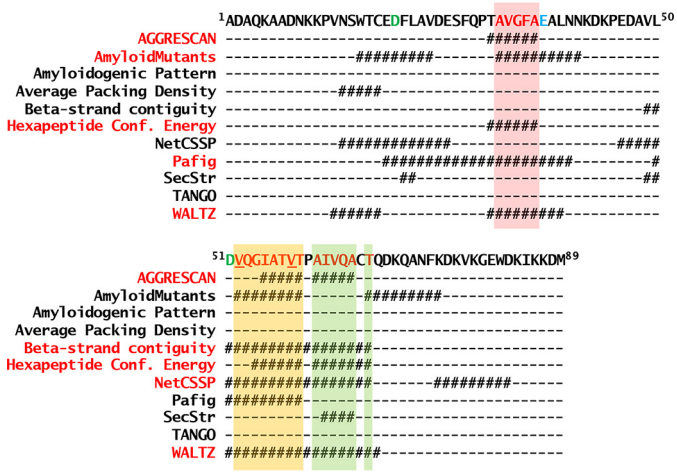

Figure 7. Prediction algorithms of amyloid core sequence regions identify potential fibrillogenic sequence regions within HdeA. The 89-amino-acid HdeA sequence was evaluated at http://aias.biol.uoa.gr/AMYLPRED2/[3] to estimate the amyloid-forming tendencies of sequence segments in HdeA. Regions that were flagged as amyloidogenic by more than five of the 11 provided algorithms are *color shaded* and represented in *red lettering* within the sequence. The specific algorithms that scored a "hit" on a given amino acid residue are listed below the amino acid sequence and denoted by the *hash symbol* (#), and the specific algorithms that contributed to the consensus of the highlighted regions are shown in *red letters* to the *left* of the figure. Each *shaded* sequence segment is mapped onto the ribbon model structure of HdeA with the corresponding color. In the amino acid sequence, the two *underlined* valine residues (Val^{52} and Val^{58}) are essential for the molecular chaperone activity of HdeA as determined by Wu *et al.* (24), and the *green lettered* residues Asp^{20} and Asp^{51} were characterized as "acid sensor" residues that dictate the denaturing transition of HdeA as determined by Foit *et al.* (30). The Glu^{37} residue denoted in *cyan* is another residue characterized by Foit *et al.* (30) as a residue that stabilizes the dimer interface of native HdeA. Structural images of HdeA (derived from Protein Data Bank (PDB) code 1dj8 (4)) were produced using UCSF Chimera (31). The algorithms used by AMYLPRED2 to evaluate the sequence are as follows: AGGRESCAN (32), AmyloidMutants (33), Amyloidogenic Pattern (34), Average Packing Density (35), β-strand contiguity (36), Hexapeptide Conformational (*Conf.*) Energy (37), NetCSSP (38), Pafig (39), SecStr (40), Waltz (41), and TANGO (42).

protonation of Glu^{37}, a residue immediately adjacent to the $^{32}AVGFA^{36}$ sequence region and a residue closely involved in the activation of the HdeA molecular chaperone activity. By performing mutation analysis of this residue, we could conceivably probe in future experiments the relationship between fibrillation of HdeA and the amino acid sequence of this protein in more detail.

The reversible fibrillation of HdeA is an example of a relatively rare phenomenon; however, very prominent examples of such reversibility exist, such as the p53 tetramerization domain (26), the repeat domain of Pmel17 (27), and the two reversible amyloid cores RAC1 and RAC2 in the LC domain of fused in sarcoma (FUS), a protein integral to the formation of RNA-enriched cellular granules (28). Interestingly, in many of the

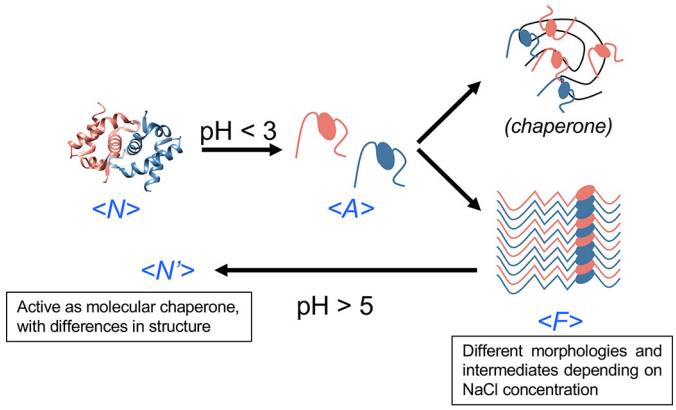

Figure 8. Graphic summary of the present study. <N> denotes the native HdeA dimer; <A> denotes the acid-induced active form. <F> denotes the atypical fibrillar form detected in this study, and <N′> denotes the soluble form of HdeA that was recovered from fibril samples that were formed at pH 2.0 by incubation at pH 7.0 and that were capable of being reactivated into the active <A> form by another shift to acidic pH. The pathway toward HdeA fibrils (<F>) differs according to the experimental conditions, notably, the concentration of NaCl.

cases above, the reversibility of the fibrillogenic reaction was utilized as a biologically relevant modulable switch that lends itself to a unique function, which has resulted in the concept of "functional amyloids." It would be intriguing if *E. coli* HdeA was also utilizing this ability to form fibrils in a presently unknown function in the bacterial periplasm or if other components of the periplasm modulate this behavior.

Fig. 8 summarizes the results of our present study. After denaturation triggered by low-pH conditions, HdeA is converted to an active chaperone that binds to acid-denatured proteins in the periplasm ("chaperone"). Under the same conditions, HdeA is also converted readily to an atypical, insoluble fibrillar form ("<F>") that is reverted to a soluble form upon another shift to neutral pH ("<N′>"). At present, we are not able to determine conclusively that HdeA is capable of returning completely to the original native structure (if <N> = <N′>) or is assuming another soluble form; the finding that this recovered form is capable of being reactivated as a molecular chaperone at low pH seems to argue for complete recovery of <N>, whereas the results of secondary structural analysis (Figs. 5 and 6) presently give conflicting data; the CD spectra argue for almost complete reversibility, whereas the ATR-FTIR experiments suggest that the reconstituted species is markedly distinct from native HdeA. Although we intend to probe this discrepancy in much more detail in further experiments, a possible explanation for the discrepancies seen in the ATR-FTIR experiments in Fig. 6 may lie in the fact that we used D_2O-hydrated lyophilized samples in these measurements; the <N′> state may be metastable and prone to reversion to the <F> state upon concentration. This outstanding question, among many other open questions, will need to be addressed in further studies.

Experimental procedures

Expression vectors and protein purification

A pET23a(+)-derived expression vector for *E. coli* HdeA was constructed by replacing the ORF of an *E. coli* GroEL expres-

Downloaded from http://www.jbc.org/ at TOTTORI UNIVERSITY on February 11, 2019

sion vector (pETEL) previously developed in our lab (29) with the ORF of the HdeA precursor sequence. This plasmid (pET23-HdeA) was used to transform JM109(DE3) cells, and transformants were further cultivated in LB medium for use in purification of HdeA.

Purification of HdeA was performed according to a protocol based upon an original procedure described by Kern *et al.* (2) where initial preparation of periplasmic extracts of *E. coli* was performed using osmotic shock followed by sequential chromatography steps using DEAE-Sephacel and hydroxyapatite. However, in our procedure, we substituted the DEAE-Sephacel anion-exchange step with an anion-exchange column chromatography step using Resource Q, developed with a linear NaCl gradient of 0–0.5 M, and we substituted the hydroxyapatite step with a cation-exchange chromatography step using Resource S based upon a modification introduced by Tapley *et al.* (11) that utilized HiTrap SP Sepharose for the second chromatography step. The buffer used in the Resource S chromatography was 20 mM sodium acetate, pH 4.0, and the column was developed using a 0–0.7 M NaCl linear gradient. All chromatography steps were performed on an ÄKTA FPLC system.

In vitro fibril formation

Monitoring of protein samples for Thio-T–positive fibril formation was performed in 20 mM glycine-HCl buffer adjusted to the relevant pH and NaCl concentrations. Protein concentrations were set to 1 mg/ml for both α-Synuclein and HdeA. Samples also contain 20 μM Thio-T to allow real-time monitoring of fibril extension by specific fluorescence. Reactions were prepared in 96-well plates, and sample incubation and sample measurements were performed using a PerkinElmer Life Sciences ARVO X4 fluorescence plate reader with agitation abilities. Samples were agitated for 15-min intervals interspersed with 10 s of fluorescence measurement at an excitation wavelength of 450 nm using an emission cutoff filter at 486 nm.

In experiments that involved a shift in the experimental pH from pH 2 to higher values (specifically Figs. 4 and 5*A*), samples were adjusted to the new pH by adding aliquots of Tris base solution to achieve the required pH. Typically, 1.6 μl of 2 M Tris base solution was sufficient to shift a 150-μl sample initially incubated at pH 2 to pH 7. Prior to the experiments, mock samples were used to estimate the concentration and amount of Tris base solution required to attain a given pH, and the actual pH of each sample was estimated visually by spotting small aliquots onto Phenol Purple (pH 3.4–6.4) or Methyl Red (pH 5.4–7.0) pH test paper (Advantec Toyo Roshi, Japan).

Transmission EM

Samples that had been monitored for Thio-T fluorescence increase as described above were diluted (10–30-fold) and applied to collodion-covered carbon mesh disks for 90 s. Excess samples were blotted off, and the sample disks were briefly rinsed by applying 5 μl of Milli-Q water and immediate blotting. Samples were next stained by application of a 15-fold–diluted solution of EM Stainer (Nisshin EM Co., Japan) for 30 s followed by blotting and air drying of the completed sample. TEM micrographs were taken on a JEOL 1400Plus electron microscope operating at 80 kV.

Gel electrophoresis of HdeA species and monitoring aggregation rescue assays of ADH

The partitioning of various HdeA samples into soluble and insoluble fractions was observed by separating the soluble and insoluble species using centrifugation for 20 min at 15,000 × *g* and subsequent analysis by 15% Laemmli SDS-PAGE. Insoluble protein was solubilized using 8 M urea when necessary. It should be noted that the results in Fig. 4*C* are not a quantitative representation of the amount of HdeA in the soluble and insoluble species as differences in concentration ratio are incorporated as a consequence of the protocol.

The ability of HdeA to prevent the acid-induced aggregation of ADH was tested by adding 10 μM ADH samples to 100 μM HdeA samples and lowering the pH of the mixture to pH 1.0 using concentrated TCA. The lower pH value in this experiment was necessary to aggregate the target ADH under these conditions. As seen in Fig. 2*C*, the ability of HdeA to form fibrils was unchanged at pH 1. Samples adjusted to pH 1.0 were incubated for 1 h at 25 °C and then observed using SDS-PAGE as outlined above.

CD spectra

For the results in Fig. 5, *A* and *B*, HdeA samples (1 mg/ml) were prepared initially at 25 °C in either 30 mM Tris-HCl buffer, pH 7.0, or 20 mM glycine-HCl buffer adjusted to the respective pH and NaCl concentrations. Before measurement, each sample was diluted 20-fold to a concentration of 50 μg/ml with Milli-Q water. Dilution using water lowered the overall absorbance of each sample and allowed reliable measurements to be made up to 190 nm. Prior to incorporating this protocol, we confirmed that the dilution step would not result in pH shifts to values higher than 4, and the results in Fig. 4*A* suggest that changes in fibril structure and morphology as a result of this shift would be unlikely. Measurements were taken in 1-mm-path quartz cells on a Jasco J-820 spectropolarimeter. Spectra are averages of eight individual scans. The secondary structural composition of each sample as suggested by the CD spectra was estimated by using an online spectrum analysis tool, BeStSel (http://bestsel.elte.hu/index.php)[3] (18, 43).

For the time-lapse scans shown in Fig. 5*C*, samples were prepared in either 150-μl aliquots in a 96-well plate (for the 150 mM NaCl samples) or in 1-ml aliquots in 13 (inner diameter) × 100-mm glass test tube (for the 0 mM NaCl samples; P-type test tube, Nichiden-Rika Glass). Test tube samples were agitated in a constant-temperature water bath. For both samples, the initial concentration of HdeA was 1 mg/ml. Before measurement, aliquots were diluted with the respective original buffers (50-fold for the 150 mM samples (HdeA concentration during measurement, 20 μg/ml) and 20-fold for the 0 mM samples (HdeA concentration during measurement, 50 μg/ml)).

AFM

AFM measurements of HdeA fibrils were performed on a Digital Instruments Nanoscope IVa at room temperature. Samples were prepared by applying 10–20 μg/ml aliquots onto freshly cleaved mica stages and incubating at room temperature for 1 h. The samples were washed by application of Milli-Q water to the stage and samples were air-dried overnight before

Downloaded from http://www.jbc.org/ at TOTTORI UNIVERSITY on February 11, 2019

measurement. Measurements were performed using a Bruker NCHV-10V cantilever in tapping mode.

ATR-FTIR

ATR-FTIR spectra were measured on a PerkinElmer Life Sciences Spectrum 65 FT-IR spectrophotometer equipped with the universal ATR sampling accessory (diamond/ZnSe crystal). Samples of HdeA in various configurations and a reference sample of α-Synuclein fibril form (~20 μg) in their respective buffers were lyophilized for ~25 h to remove water and first measured directly on the apparatus to estimate the absorbance of the sample. Eight scans (4 cm^{-1} resolution) with CO_2/H_2O atmospheric suppression applied were averaged. Next, 2 μl of 99.9% D_2O (Cambridge Isotope Laboratories) was added directly onto the samples, and pressure was reapplied. After a 5-min incubation, the samples were remeasured to obtain the spectra shown in Fig. 6. The analysis functions of the software package (Spectrum version 10.03.09) were used to obtain second derivative spectra (number of data points used as analysis window: 5).

Author contributions—S. M. and T. M. conceptualization; S. M., Y. U., Y. K., and T. M. formal analysis; S. M. and Y. U. investigation; K. H., Y. K., and T. M. data curation; K. H. methodology; K. H., Y. K., and T. M. writing-review and editing; Y. K. and T. M. funding acquisition; Y. K. validation; T. M. writing-original draft; T. M. project administration.

Acknowledgments—We are grateful to Professors Hiroyuki Saimoto, Shinsuke Ifuku, and Dr. Hironori Izawa of Tottori University for allowing us to use the FT-IR spectrophotometer. We also thank Hanae Yamamoto and Naoya Fukui of our laboratory for providing reference α-Synuclein fibril samples for CD and ATR-FTIR analysis.

References

1. Gorden, J., and Small, P. L. (1993) Acid resistance in enteric bacteria. *Infect. Immun.* **61,** 364–367 Medline
2. Kern, R., Malki, A., Abdallah, J., Tagourti, J., and Richarme, G. (2007) *Escherichia coli* HdeB is an acid stress chaperone. *J. Bacteriol.* **189,** 603–610 CrossRef Medline
3. Yang, F., Gustafson, K. R., Boyd, M. R., and Wlodawer, A. (1998) Crystal structure of *Escherichia coli* HdeA. *Nat. Struct. Biol.* **5,** 763–764 CrossRef Medline
4. Gajiwala, K. S., and Burley, S. K. (2000) HDEA, a periplasmic protein that supports acid resistance in pathogenic enteric bacteria. *J. Mol. Biol.* **295,** 605–612 CrossRef Medline
5. Wang, W., Rasmussen, T., Harding, A. J., Booth, N. A., Booth, I. R., and Naismith, J. H. (2012) Salt bridges regulate both dimer formation and monomeric flexibility in HdeB and may have a role in periplasmic chaperone function. *J. Mol. Biol.* **415,** 538–546 CrossRef Medline
6. Malki, A., Le, H. T., Milles, S., Kern, R., Caldas, T., Abdallah, J., and Richarme, G. (2008) Solubilization of protein aggregates by the acid stress chaperones HdeA and HdeB. *J. Biol. Chem.* **283,** 13679–13687 CrossRef Medline
7. Dahl, J. U., Koldewey, P., Salmon, L., Horowitz, S., Bardwell, J. C., and Jakob, U. (2015) HdeB functions as an acid-protective chaperone in bacteria. *J. Biol. Chem.* **290,** 65–75 CrossRef Medline
8. Yoshida, T., Ueguchi, C., Yamada, H., and Mizuno, T. (1993) Function of the *Escherichia coli* nucleoid protein, H-NS: molecular analysis of a subset of proteins whose expression is enhanced in a hns deletion mutant. *Mol. Gen Genet.* **237,** 113–122 Medline
9. Hong, W., Jiao, W., Hu, J., Zhang, J., Liu, C., Fu, X., Shen, D., Xia, B., and Chang, Z. (2005) Periplasmic protein HdeA exhibits chaperone-like activity exclusively within stomach pH range by transforming into disordered conformation. *J. Biol. Chem.* **280,** 27029–27034 CrossRef Medline
10. Zhang, S., He, D., Yang, Y., Lin, S., Zhang, M., Dai, S., and Chen, P. R. (2016) Comparative proteomics reveal distinct chaperone-client interactions in supporting bacterial acid resistance. *Proc. Natl. Acad. Sci. U.S.A.* **113,** 10872–10877 CrossRef Medline
11. Tapley, T. L., Körner, J. L., Barge, M. T., Hupfeld, J., Schauerte, J. A., Gafni, A., Jakob, U., and Bardwell, J. C. (2009) Structural plasticity of an acid-activated chaperone allows promiscuous substrate binding. *Proc. Natl. Acad. Sci. U.S.A.* **106,** 5557–5562 CrossRef Medline
12. Tapley, T. L., Franzmann, T. M., Chakraborty, S., Jakob, U., and Bardwell, J. C. (2010) Protein refolding by pH-triggered chaperone binding and release. *Proc. Natl. Acad. Sci. U.S.A.* **107,** 1071–1076 CrossRef Medline
13. Yu, X. C., Yang, C., Ding, J., Niu, X., Hu, Y., and Jin, C. (2017) Characterizations of the interactions between *Escherichia coli* periplasmic chaperone HdeA and its native substrates during acid stress. *Biochemistry* **56,** 5748–5757 CrossRef Medline
14. Fukui, N., Araki, K., Hongo, K., Mizobata, T., and Kawata, Y. (2016) Modulating the effects of the bacterial chaperonin GroEL on fibrillogenic polypeptides through modification of domain hinge architecture. *J. Biol. Chem.* **291,** 25217–25226 CrossRef Medline
15. Ojha, B., Fukui, N., Hongo, K., Mizobata, T., and Kawata, Y. (2016) Suppression of amyloid fibrils using the GroEL apical domain. *Sci. Rep.* **6,** 31041 CrossRef Medline
16. Uversky, V. N., Li, J., and Fink, A. L. (2001) Evidence for a partially folded intermediate in α-synuclein fibril formation. *J. Biol. Chem.* **276,** 10737–10744 CrossRef Medline
17. Vassar, P. S., and Culling, C. F. (1959) Fluorescent stains, with special reference to amyloid and connective tissues. *Arch. Pathol.* **68,** 487–498 Medline
18. Micsonai, A., Wien, F., Bulyáki, É., Kun, J., Moussong, É., Lee, Y. H., Goto, Y., Réfrégiers, M., and Kardos, J. (2018) BeStSel: a web server for accurate protein secondary structure prediction and fold recognition from the circular dichroism spectra. *Nucleic Acids Res.* **46,** W315–W322 CrossRef Medline
19. Goormaghtigh, E., Cabiaux, V., and Ruysschaert, J. M. (1990) Secondary structure and dosage of soluble and membrane proteins by attenuated total reflection Fourier-transform infrared spectroscopy on hydrated films. *Eur. J. Biochem.* **193,** 409–420 CrossRef Medline
20. Waterman, S. R., and Small, P. L. (1996) Identification of sigma S-dependent genes associated with the stationary-phase acid-resistance phenotype of *Shigella flexneri*. *Mol. Microbiol.* **21,** 925–940 CrossRef Medline
21. Lazar, K. L., Miller-Auer, H., Getz, G. S., Orgel, J. P., and Meredith, S. C. (2005) Helix-turn-helix peptides that form α-helical fibrils: turn sequences drive fibril structure. *Biochemistry* **44,** 12681–12689 CrossRef Medline
22. Tayeb-Fligelman, E., Tabachnikov, O., Moshe, A., Goldshmidt-Tran, O., Sawaya, M. R., Coquelle, N., Colletier, J. P., and Landau, M. (2017) The cytotoxic Staphylococcus aureus PSMα3 reveals a cross-α amyloid-like fibril. *Science* **355,** 831–833 CrossRef Medline
23. Tsolis, A. C., Papandreou, N. C., Iconomidou, V. A., and Hamodrakas, S. J. (2013) A consensus method for the prediction of 'aggregation-prone' peptides in globular proteins. *PLoS One* **8,** e54175 CrossRef Medline
24. Wu, Y. E., Hong, W., Liu, C., Zhang, L., and Chang, Z. (2008) Conserved amphiphilic feature is essential for periplasmic chaperone HdeA to support acid resistance in enteric bacteria. *Biochem. J.* **412,** 389–397 CrossRef Medline
25. Salmon, L., Stull, F., Sayle, S., Cato, C., Akgül, Ş., Foit, L., Ahlstrom, L. S., Eisenmesser, E. Z., Al-Hashimi, H. M., Bardwell, J. C. A., and Horowitz, S. (2018) The mechanism of HdeA unfolding and chaperone activation. *J. Mol. Biol.* **430,** 33–40 CrossRef Medline
26. Lee, A. S., Galea, C., DiGiammarino, E. L., Jun, B., Murti, G., Ribeiro, R. C., Zambetti, G., Schultz, C. P., and Kriwacki, R. W. (2003) Reversible amyloid formation by the p53 tetramerization domain and a cancer-associated mutant. *J. Mol. Biol.* **327,** 699–709 CrossRef Medline

Downloaded from http://www.jbc.org/ at TOTTORI UNIVERSITY on February 11, 2019

ASBMB

27. McGlinchey, R. P., and Lee, J. C. (2018) Why study functional amyloids? Lessons from the repeat domain of Pmel17. *J. Mol. Biol.* **430,** 3696–3706 CrossRef Medline
28. Luo, F., Gui, X., Zhou, H., Gu, J., Li, Y., Liu, X., Zhao, M., Li, D., Li, X., and Liu, C. (2018) Atomic structures of FUS LC domain segments reveal bases for reversible amyloid fibril formation. *Nat. Struct. Mol. Biol.* **25,** 341–346 CrossRef Medline
29. Machida, K., Fujiwara, R., Tanaka, T., Sakane, I., Hongo, K., Mizobata, T., and Kawata, Y. (2009) Gly192 at hinge 2 site in the chaperonin GroEL plays a pivotal role in the dynamic apical domain movement that leads to GroES binding and efficient encapsulation of substrate proteins. *Biochim. Biophys. Acta* **1794,** 1344–1354 CrossRef Medline
30. Foit, L., George, J. S., Zhang, B. W., Brooks, C. L., 3rd, and Bardwell, J. C. (2013) Chaperone activation by unfolding. *Proc. Natl. Acad. Sci. U.S.A.* **110,** E1254–E1262 CrossRef Medline
31. Pettersen, E. F., Goddard, T. D., Huang, C. C., Couch, G. S., Greenblatt, D. M., Meng, E. C., and Ferrin, T. E. (2004) UCSF Chimera—a visualization system for exploratory research and analysis. *J. Comput. Chem.* **25,** 1605–1612 CrossRef Medline
32. Conchillo-Solé, O., de Groot, N. S., Avilés, F. X., Vendrell, J., Daura, X., and Ventura, S. (2007) AGGRESCAN: a server for the prediction and evaluation of "hot spots" of aggregation in polypeptides. *BMC Bioinformatics* **8,** 65 CrossRef Medline
33. O'Donnell, C. W., Waldispühl, J., Lis, M., Halfmann, R., Devadas, S., Lindquist, S., and Berger, B. (2011) A method for probing the mutational landscape of amyloid structure. *Bioinformatics* **27,** i34–42 CrossRef Medline
34. López de la Paz, M., and Serrano, L. (2004) Sequence determinants of amyloid fibril formation. *Proc. Natl. Acad. Sci. U.S.A.* **101,** 87–92 CrossRef Medline
35. Galzitskaya, O. V., Garbuzynskiy, S. O., and Lobanov, M. Y. (2006) Prediction of amyloidogenic and disordered regions in protein chains. *PLoS Comput. Biol.* **2,** e177 CrossRef Medline
36. Zibaee, S., Makin, O. S., Goedert, M., and Serpell, L. C. (2007) A simple algorithm locates β-strands in the amyloid fibril core of α-synuclein, Aβ, and tau using the amino acid sequence alone. *Protein Sci.* **16,** 906–918 CrossRef Medline
37. Zhang, Z., Chen, H., and Lai, L. (2007) Identification of amyloid fibril-forming segments based on structure and residue-based statistical potential. *Bioinformatics* **23,** 2218–2225 CrossRef Medline
38. Kim, C., Choi, J., Lee, S. J., Welsh, W. J., and Yoon, S. (2009) NetCSSP: web application for predicting chameleon sequences and amyloid fibril formation. *Nucleic Acids Res.* **37,** W469–W473 CrossRef Medline
39. Tian, J., Wu, N., Guo, J., and Fan, Y. (2009) Prediction of amyloid fibril-forming segments based on a support vector machine. *BMC Bioinformatics* **10,** Suppl. 1, S45 CrossRef Medline
40. Hamodrakas, S. J., Liappa, C., and Iconomidou, V. A. (2007) Consensus prediction of amyloidogenic determinants in amyloid fibril-forming proteins. *Int. J. Biol. Macromol.* **41,** 295–300 CrossRef Medline
41. Maurer-Stroh, S., Debulpaep, M., Kuemmerer, N., Lopez de la Paz, M., Martins, I. C., Reumers, J., Morris, K. L., Copland, A., Serpell, L., Serrano, L., Schymkowitz, J. W., and Rousseau, F. (2010) Exploring the sequence determinants of amyloid structure using position-specific scoring matrices. *Nat. Methods* **7,** 237–242 CrossRef Medline
42. Fernandez-Escamilla, A. M., Rousseau, F., Schymkowitz, J., and Serrano, L. (2004) Prediction of sequence-dependent and mutational effects on the aggregation of peptides and proteins. *Nat. Biotechnol.* **22,** 1302–1306 CrossRef Medline
43. Micsonai, A., Wien, F., Kernya, L., Lee, Y. H., Goto, Y., Réfrégiers, M., and Kardos, J. (2015) Accurate secondary structure prediction and fold recognition for circular dichroism spectroscopy. *Proc. Natl. Acad. Sci. U.S.A.* **112,** E3095–E3103 CrossRef Medline

Downloaded from http://www.jbc.org/ at TOTTORI UNIVERSITY on February 11, 2019

Acid-denatured small heat shock protein HdeA from *Escherichia coli* forms reversible fibrils with an atypical secondary structure

Shiori Miyawaki, Yumi Uemura, Kunihiro Hongo, Yasushi Kawata and Tomohiro Mizobata

J. Biol. Chem. 2019, 294:1590-1601.
doi: 10.1074/jbc.RA118.005611 originally published online December 10, 2018

Access the most updated version of this article at doi: 10.1074/jbc.RA118.005611

Alerts:
- When this article is cited
- When a correction for this article is posted

Click here to choose from all of JBC's e-mail alerts

This article cites 43 references, 15 of which can be accessed free at
http://www.jbc.org/content/294/5/1590.full.html#ref-list-1

Downloaded from http://www.jbc.org/ at TOTTORI UNIVERSITY on February 11, 2019